



Towards a predictive thermal explosion model for energetic materials*

JACK J. YOH[†], MATTHEW A. MCCLELLAND, JON L. MAIENSCHEIN and
JEFFREY F. WARDELL

*Energetic Materials Center, Lawrence Livermore National Laboratory, University of California, P.O.Box 808,
Livermore, CA 94551, U.S.A.*

Received ; Accepted

Abstract. We present an overview of models and computational strategies for simulating the thermal response of high explosives using a multi-physics hydrodynamics code, ALE3D. Recent improvements to the code have aided our computational capability in modeling the behavior of energetic materials systems exposed to strong thermal environments such as fires. We apply these models and computational techniques to a thermal explosion experiment involving the slow heating of a confined explosive. The model includes the transition from slow heating to rapid deflagration in which the time scale decreases from days to hundreds of microseconds. Thermal, mechanical, and chemical effects are modeled during all phases of this process. The heating stage involves thermal expansion and decomposition according to an Arrhenius kinetics model while a pressure-dependent burn model is employed during the explosive phase. We describe and demonstrate the numerical strategies employed to make the transition from slow to fast dynamics. In addition, we investigate the sensitivity of wall expansion rates to numerical strategies and parameters. Results from a one-dimensional model show that violence is influenced by the presence of a gap between the explosive and container. In addition, a comparison is made between 2D model and measured results for the explosion temperature and tube wall expansion profiles.

Keywords: arbitrarily Lagrangian Eulerian, variable mass scaling, multi-materials, high-explosive modeling, cookoff, deflagration, PBXN-109

1. Introduction

In the DoD/DOE community, there is an interest in using computer simulations to reduce the number of experiments for weapons design and safety evaluation. One area of great success in modeling and simulation is the characterization of munitions exposed to extreme conditions, such as shocks and detonations [1, 2, 3]. Hydrocodes, which are designed to simulate the high-frequency response involving initiation and propagation of shocks and detonations, have been used extensively by the energetic materials community [4, 5, 6, 7, 8, 9].

On the other hand, models and numerical strategies are still being developed for the slow heating of energetic materials until reaction (cookoff) [10–16]. The Navy is interested in the behavior of munitions in shipboard fires to help with the design of storage systems and the development of fire fighting strategies. In these fires, time scales for behavior can range from days to microseconds. During the relatively slow heating phase, the response of an energetic

*Approved for public release; distribution is unlimited. The work was performed under the auspices of the U.S. Department of Energy by the University of California, Lawrence Livermore National Laboratory under Contract No. W-7405-Eng-48.

[†]Corresponding author. Electronic mail: yoh1@llnl.gov

materials system is paced by thermal diffusion and chemical decomposition, while the mechanical response is essentially a quasi-static process. As the decomposition reactions accelerate, heat is generated faster than it can diffuse. Product gases are formed and the resulting pressure rises accelerate the energetic and containment material response. The resulting thermal explosion can range in violence from a pressure rupture to a detonation.

A number of investigators have modeled slow cookoff experiments. Chidester *et al.* [17] calculated explosion times for HMX- and TATB-based explosives subjected to varying confinement and thermal environments. Tarver and Tran [18] improved thermal decomposition models for HMX-based plastic bonded explosives and attained reasonable predictions for ignition time using the thermal-chemical code, Chemical TOPAZ. Moving beyond predictions of time-to-event to violence of reaction required model development and characterization of heated explosives. Earlier models were evaluated against small-scale tests (see [14, 19–21]). It was recognized that the models required further development and needed to be validated against benchmark cookoff experiments (see [13, 22, 23]). More recent modeling efforts have focused on wall strain rates as a measure of cookoff violence. Erikson *et al.* [24] used a suite of codes to model the two separate phases of the cookoff process. The information obtained from their pre-ignition calculation was used to initialize the post-ignition simulation for predicting the wall expansion.

In the modeling work of this study, the process of cookoff is not separated into two regimes. Instead, a single calculation is performed for the heating, ignition, and explosive phases of cookoff. Coupled thermal, mechanical, and chemical models are used during all of these stages to account for effects such as chemical decomposition, burning, thermal expansion, and the closing of gaps. In the future, we will include thermally-formed cracks and porosity in the explosive along with gas flow through this material. It is seen that the modeling of thermal explosions requires computational tools and models that can handle a wide variety of physical processes and time scales.

For the purpose of illustration and to help us develop a conceptual framework, we consider the energetic material, PBXN-109, (64% RDX, 20% Al, 16% DOA/HTPB). Because of the relatively low content of RDX and the presence of an inactive binder, PBXN-109 is a relatively insensitive high explosive.

In this paper, we describe how the cookoff modeling and simulation are done with the Arbitrarily Lagrangian-Eulerian code [25, 26], ALE3D. In particular, we discuss the numerical methodology to transition from slow to fast time scales. We apply our modeling capability to a Scaled Thermal Explosion Experiment (STEX) [13] and compare calculated and measured curves for the wall strain during both the heating and explosive phases of the test. Highly resolved calculations show very rich behavior for this cookoff test.

2. Description of the thermal explosion experiment

The STEX is designed to quantify the violence of thermal explosions under carefully controlled conditions, and to provide a database which we can use to validate predictive codes and models [13]. A cylindrical test, shown in Figure 1, is devised where the ignition starts in the axially central region of the cylinder. The confinement vessel consists of a steel wall and heavily reinforced end caps which confine the decomposition gases until the tube wall fails. A constant length to diameter ratio of 4:1 is used. For a charge of 5.08 cm diameter, 20.3 cm length, the respective wall thickness was 0.4 cm, giving an approximate confinement pressure

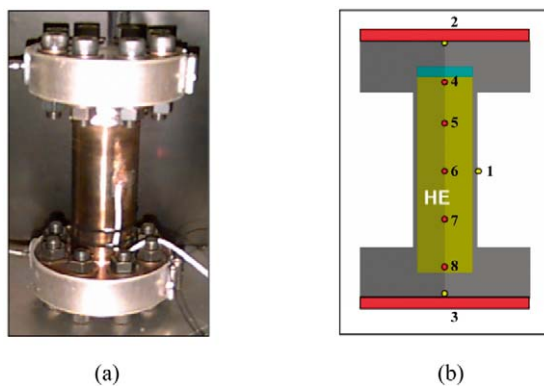


Figure 1. (a) Photograph of the STEX vessel. (b) Schematic of the ALE3D model domain.

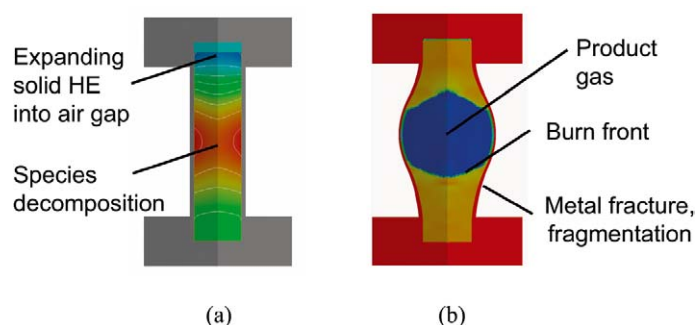


Figure 2. (a) Pre-ignition characterized by slow thermo-chemical decomposition of HE. (b) Post-ignition illustrated with rapid burn propagation due to expanding hot product gases.

of 200 MPa. A 5% gap is provided in the upper part of the vessel to allow the high explosive (HE) to expand freely before ignition. A feedback control system is used to adjust three radiant heaters to control the wall temperature at location no. 1 of Figure 1(b). The thermocouples at location nos. 2 and 3 on the end caps are controlled with separate control loops.

3. Model for PBXN-109

In this model, the solid explosive decomposes volumetrically as it is heated to generate product gases (see Figure 2(a)). These reactions accelerate to a point at which the HE ignites and burns. A burn front then moves as a sheet away from the ignition point (see Figure 2(b)). Partially decomposed HE is converted to products as the burn front propagates.

The behavior of the explosive and container are described with continuum models for the transport of momentum, energy, and chemical species. The momentum balance accounts for acceleration and the mechanical response of the solids, gases, and mixtures of these materials. The time-dependent energy balance includes convection, conduction, mechanical work, and heat generated by chemical reaction. The chemical species are transported by convection, but diffusion is assumed to be negligible.

The decomposition of PBXN-109 is modeled by three-step, four-species chemical kinetics based on the pure RDX model reported in [27]. The mechanical models for the solid chemical constituents along with the steel components are taken to have Steinberg-Guinan [28] strength models in which a polynomial expression is used for the equations of state. The gaseous

Table 1. Material properties used in the cookoff simulation. Shown are the density (ρ), coefficient of thermal expansion (CTE), shear modulus (μ), and yield strength (Y_0) at 20 °C and 10^5 Pa.

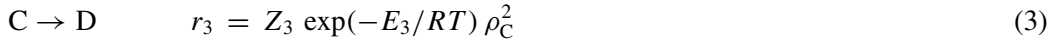
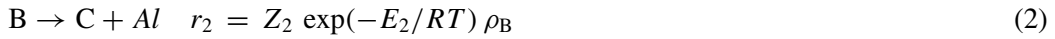
	ρ (g/cm ³)	CTE (°C ⁻¹)	μ (GPa)	Y_0 (GPa)
PBXN-109	1.67	1.21e-4	4.628e-3	0.06
Steel 4340	7.83	1.20e-5	77.0	1.03

Table 2. Chemical kinetics parameters for decomposition of PBXN-109

Reaction step	$\ln Z_k$	E_k (kJ/g-mole-°K)	q_k (J/g)
A \rightarrow B	43.84 s ⁻¹	194.7	268.0 (endothermic)
B \rightarrow C + Al	39.04 s ⁻¹	182.5	-803.9 (exothermic)
C \rightarrow D	32.84 cm ³ /s-g	141.1	-4241.2 (exothermic)

products are treated as no-strength materials with gamma-law equations of state. The thermal conductivity for the HE solid species is taken to be constant, whereas the effects of temperature are included for the gaseous species. The air in the gaps between the HE and the steel case is modeled with a gamma-law model. The parameters in these models were determined from measurements as reported in [10, 11] (see Table 1).

The three-step, four-species reaction mechanism for PBXN-109 is



where A and B are solid species, and C and D are product gases. In the second reaction step, aluminum, Al, is separated from the reactant B without reacting. The rate parameters above are adjusted to fit One-Dimensional-Time-to-Explosion (ODTX) measurements [29], and they are given in Table 2.

The time-to-explosion measurements are made using a standard ODTX apparatus in which the outer surface of a 1.27 cm diameter HE sphere is suddenly increased to a higher set-point temperature. The time to explosion is the time elapsed from the start of heating until confinement failure. The measured and calculated ODTX results for PBXN-109 are shown in Figure 3(a). The measurements include values for the sample of this study and results from an earlier study [30]. The model includes chemical reaction and thermal transport without material motion. The data is well represented by the model, except for temperatures above 235 °C.

After the chemical reactions have progressed significantly into the faster regime of cookoff in which changes are occurring on the time scale of the sound speed, a switch is made to a

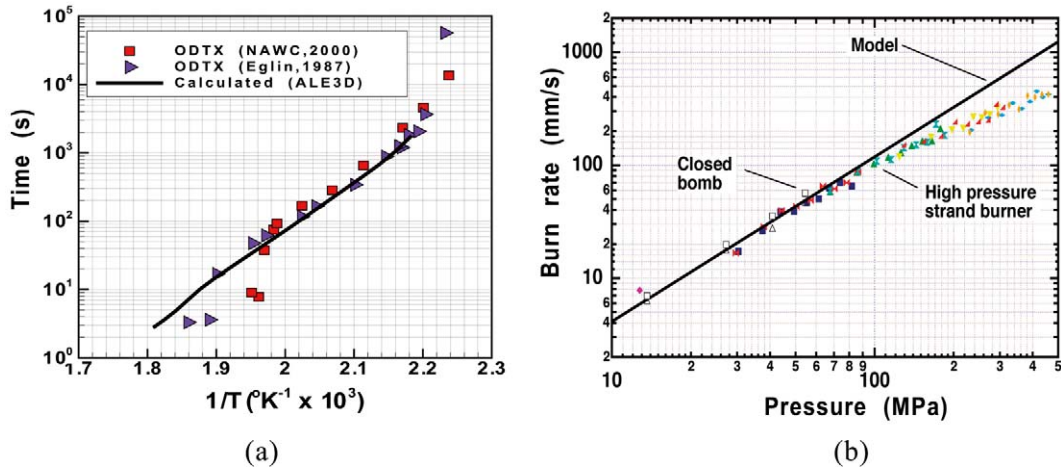


Figure 3. (a) Measured and calculated ODTX results for PBXN-109. (b) Measured and modeled burn rate data for PBXN-109 sample.

burn front model in which reactants are converted to products in a single reaction step. The burn front velocity, V is assumed to be a function of pressure only, and it takes the form

$$V = a P^n \quad (4)$$

where V is in mm/s and P is in MPa. The parameters used in the current simulation are:

$$a = 0.146 \text{ mm/s}, \quad n = 1.45$$

This model provides a satisfactory representation of burn rates measured by Atwood [31] and Maienschein [12]. The latter results were measured in the LLNL High Pressure Strand Burner [32]. A strand of explosive (0.64 cm D × 5.7 cm L) is placed in a high pressure vessel, and is ignited at one end. Wires placed in the sample track the progress of the burn while pressure measurements are made. Figure 3(b) shows the burn rate data for the PBXN-109 sample.

4. Numerical Strategy for Cookoff Simulations

Figure 4 shows one and two-dimensional modeling domains for a STEX test. A wedge slice is taken from the center line of the STEX system shown in the right image. This one-dimensional wedge represents an axisymmetric section of the STEX system in which variations occur only in the radial direction. This approach is taken to minimize the number of three-dimensional zones needed to represent an axisymmetric domain. The boundaries at two planes of constant θ are rigid slip surfaces. In the experiment [13], the HE, nominally 5.08 cm diameter is encased in a 0.4 cm thick steel cylinder. The 5% ullage by volume is located at the outside radius of the HE in the 1D model. The gaps are treated in two different ways in the 2D models. In Model 2Da, a 4% gap by volume is included at the top end of the cylindrical charge, and a 1% gap is used at the outside radius of the HE. In Model 2Db, a 5% gap is included at the top of the cylinder, and there is no gap on the side.

The three heaters were modeled as uniform heat flux surfaces on the tube wall and top and bottom surfaces for the end caps (see Figure 1). Model Proportional-Integral-Derivative (PID) controllers were used to keep the three control temperatures near their set-point values.

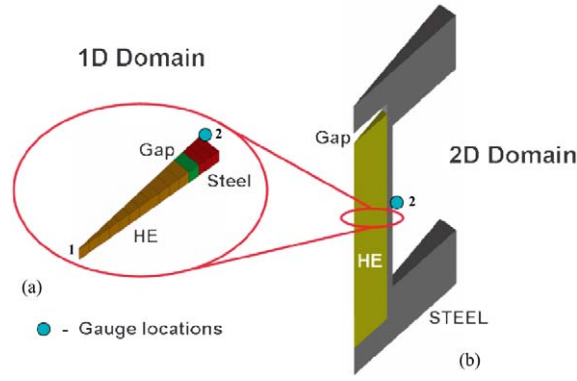


Figure 4. Schematics of 1D and 2D domains. 1D mesh is generated from a slice along the center radial line of 2D mesh on the right column. In both, a 5% gap (by volume) is present between the HE and the steel casing.

Expressions for heat transfer coefficients were applied at all outward facing surfaces of the capped tube to account for the effects of free convection and thermal radiation heat losses to the surroundings [33]. A more refined boundary-layer expression for heat transfer is used at the tube wall to account for spatial variations resulting from the rising warm air. The heat transfer is high near the lower end of the tube wall and decreases up the tube wall as the boundary layer of warm air forms and increases in thickness.

The cookoff simulation starts with a gradual increase of the set-point temperature at location no. 1 in Figure 1(b) to 130 °C, followed by a hold for 5 hours, and then an increase at a rate of 1 °C/h until cookoff. The upper (no. 2) and lower (no. 3) control thermocouples were kept 4 and 9 °C lower, respectively than the tube control TC in an effort to place the ignition point in the center of the HE. As the PBXN-109 is heated, it thermally expands to fill in the gap. At a temperature above 130 °C, exothermic decomposition begins and eventually ignition occurs near the midplane of the system. On a time scale of microseconds, the propagation of flame through the PBXN-109 causes the temperature and pressure to rise, and ultimately causes a break in confinement.

In the simulations, four different mesh resolutions (1X, 2X, 4X, 8X) are considered. In the base case (1X), there are 12 elements across the HE in the radial direction, and in the fine mesh case (8X) there are 96 elements in this direction.

4.1. MODELS FOR DYNAMIC GAPS

In real systems, there are gaps present between the HE sample and its case. Whether the presence of gaps is by design or not, its effect in the cookoff violence is believed to be significant. It is important to treat gaps or voids in all calculations related to cookoff. The ALE3D code has two ways of modeling gaps. The first way uses a standard sliding contact algorithm that makes use of the concept of master-slave surfaces. Here finite element boundaries coincide with phase boundaries, and the gap surfaces are explicitly ‘tracked.’ The second way of treating gaps is the mixed element approach that we use in this work. Interfaces pass through the middle of mixed elements that do not necessarily move with the interface. The interface is resolved on the length scale of this element. Although less accurate, this approach avoids mesh tracking and entanglement problems. The mixed-element approach can provide results of satisfactory accuracy with sufficient mesh resolution.

The mixing rules for mechanical behavior are particularly important for gaps that close. The algorithms of this study were devised with the assumption that the HE/air interface is parallel to the case wall which is generally valid except at corners of the explosive. Mechanical properties in the mixed zone are weighted in favor of the air in the gap. In the vicinity of this interface, strains normal to the interface are very small for the HE and relatively large for the air in the gap.

4.2. TIME INTEGRATION METHOD AND MASS SCALING

The equations of mass, momentum, energy, and chemistry are solved on the long time scale of the heating phase and on the short time scale of the thermal runaway phase in a single simulation. The momentum equation is integrated explicitly during both the slow and fast phases. In order to provide computationally feasible step sizes, the method of variable mass scaling [34] is applied during the slow heating phase. The density is increased in the momentum equation to reduce the sound speed and allow larger step sizes consistent with the Courant condition. However, if the time step size and material density are too large, spurious fluctuations, characteristic of a simple harmonic oscillator, appear. Thus, a tradeoff is required between numerical efficiency and accuracy. In practice, the time step size is fixed during the slow heating phase with the density calculated from the Courant condition. As the mesh is refined, the time-step size is reduced to keep the mass scaling and the sound speed at nearly constant values.

During the transition phase in which the decomposition reactions are accelerating, the time step size is reduced to meet error specifications for the calculation of thermal and composition fields. At the same time, the artificial density is reduced following the Courant condition until the physical value is obtained. When the HE reaches a user-specified temperature, the Arrhenius kinetics expression is replaced by a burn model. A level-set method is used in the modeling of the advancing burn front.

We use the Backward Euler method for the integration of the thermal equations and reaction kinetics during the heating, and transition phases. During the slow heating phase, the time step size is the value selected for the integration of the hydrodynamic equations. A switch is made to an explicit method when the time step size is a user-specified multiple of the Courant time step size calculated with no mass scaling.

5. Results and discussion

5.1. EXPERIMENTAL RESULTS

A thermal explosion experiment was performed for PBXN-109 confined in the 4130 steel vessel shown in Figure 1(a). The system was heated from room temperature to 50 °C at a rate of 3.35 °C/h, followed by a 1.67 hour hold at this temperature. Then at a ramp rate of 3.77 °C/h, the system temperature rose to 130 °C, followed by a 5 hour hold (see Figure 5). During the final heating phase, a rate of 1 °C/h was maintained for control thermocouple no. 1 until explosion (see Figure 1(b)). This slow ramp rate was selected to insure ignition near the symmetry axis. The top (no. 2) and bottom (no. 3) thermocouples were maintained at lower temperatures to give ignition at the axial midplane. Based on measured temperature profiles, ignition occurred near the middle internal thermocouple (no. 6). The control temperature (no. 1) at ignition was 152 °C. The violence of the explosion was relatively mild based on

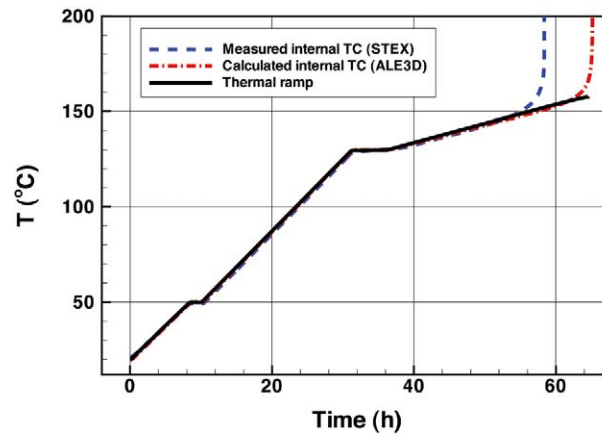


Figure 5. Calculated thermal response of confined HE in a 2D STEX experiment. The control and internal thermocouples are located at positions nos. 1 and 6 in Figure 1(b), respectively. The predicted ignition temperature is 5 degrees higher than the STEX result. Model 2Da is used with the 8X mesh.

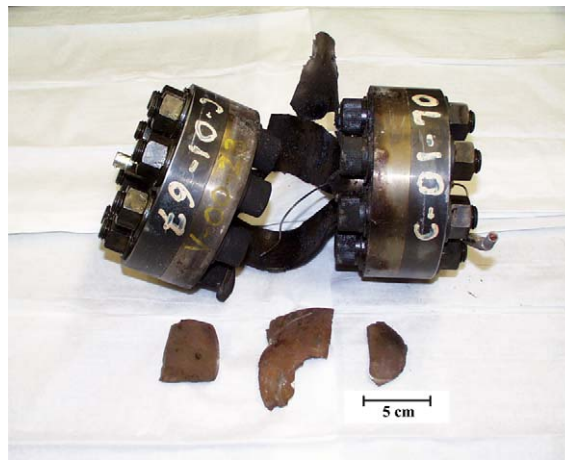


Figure 6. Post shot result showing the collected fragments.

the several hundred microsecond time scale of the measure expansion which is described below. Also the steel fragments were of the length scale 3–5 cm, indicating mild violence (see Figure 6). In comparison, the expansion in a very violent event such as a detonation would be of the time scale of a few microseconds and the steel fragments would be much smaller. Based on this evidence, this thermal explosion test involved a deflagration and not a detonation. In the following sections we compare model results with measurements made during the test.

5.2. ONE-DIMENSIONAL ANALYSIS

Although measurements cannot be compared directly with model results for the one-dimensional geometry of Figure 4(a), this geometry can be used to efficiently explore many of the important features of the thermal explosion models and provide very good estimates of numerical accuracy. The system was heated using the temperature profile described above for control thermocouple no. 1 of Figure 1(b). The explosive expands radially into the gap, decomposes, and ignites near the symmetry axis. The burn front advances outward into the

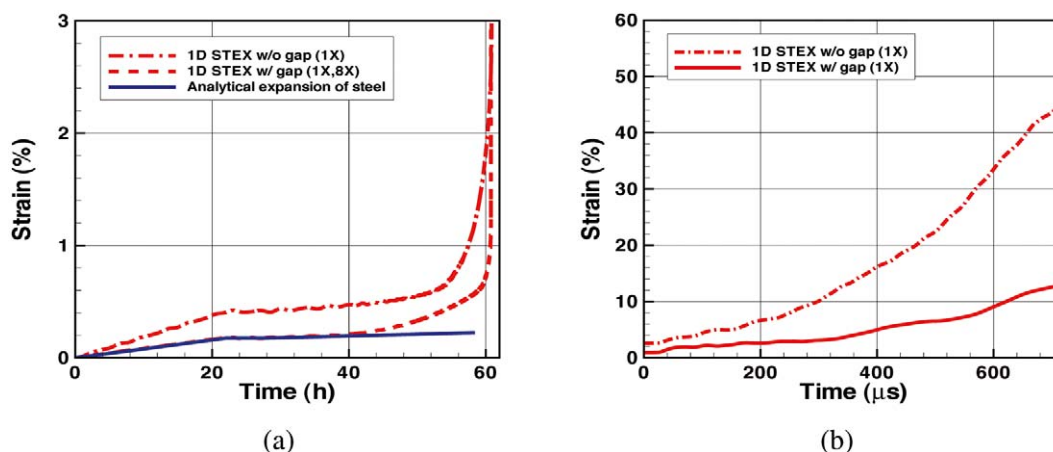


Figure 7. Simulated mechanical response of confined explosive in a 1D STEX model. The wall hoop strain is at location no. 2 in Figure 4(a). (a) Slow heating phase: the strain calculation with a gap agrees with the empty vessel result until about 40 hours as chemical decomposition of PBXN-109 becomes pronounced in the confined system. (b) Fast burn phase: the system with gap shows significantly slower strain rates than the system without gap.

relatively cold solid explosive. The resulting high pressure product gases drive the steel case outward.

Calculated results for the wall hoop strain at location no. 2 of Figure 4(a) are shown in Figure 7(a) for the one-dimensional STEX model. For comparison, the theoretical thermal expansion of an empty steel vessel is shown in the same plot. We calculate strains for systems with and without a 5% gap. In the figure, the strains are higher for the case without a gap during the slow thermal phase. The resulting strain when a gap is included (shown in dashed line) is smaller by a factor of two or more during the same time period. The strain curve for the case without a gap coincides with the analytical expansion of pure steel (shown in solid line) up to about 40 hours. As the temperature increases, the HE thermally expands inside the steel vessel at a rate approximately 10X greater than the steel vessel itself (see Table 1). An estimated time of contact at which inert PBXN-109 fills the 5% gap and starts pushing on the steel wall is approximately 53 hours. Since the solid HE undergoes chemical decomposition and the decomposition gases pressurize the vessel, the overall strain values are greater than the analytical expansion of the steel vessel alone. The effects of mesh refinement on the strain curves were determined to be negligible during the slow heating phase, since the curves for the 1X and 8X meshes are very similar.

In Figure 8(a), we plot the pressure rise at location no. 1 of Figure 4(a) for the case with no gap in the 1D STEX system. During the first 40 hours, the system with a gap experiences no significant pressure increase. This observation supports the claim that the presence of gaps in the STEX system can prevent unwanted over pressurization of the vessel before the ignition takes place. After 40 hours, PBXN-109 continues to undergo chemical decomposition, producing more product gases that further pressurize the vessel. The increased production of the first gaseous species at location no. 1 of Figure 4(a), X_C , is tied in with the rapid pressure rise in the system as seen from Figure 8(b). As solid HE species (X_A , X_B) are consumed to generate more hot product gases (X_C , X_D), the pressure as calculated by the gamma-law model, starts to increase significantly. At about 62 hours, well into the cookoff phase, both the elevated temperature ($> 2000^\circ\text{K}$) and the presence of final product gas (X_D) trigger the switching of

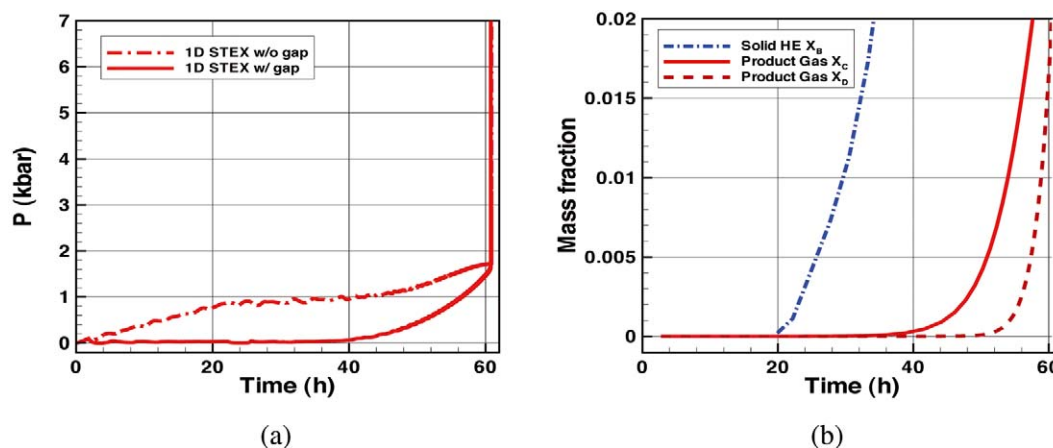


Figure 8. (a) The pressures at location no. 1 of Figure 4(a) starts to rise above values for inert systems at around 40 hours. (b) Formation of gaseous product X_C at location no. 1 of Figure 4(a) about 40 hours marks the onset of pressure increase in the 1D STEX system with gap. 8X mesh is used.

chemical kinetics to a deflagration burn-front mechanism that rapidly expands the steel vessel during the ignition-burn phase.

Figure 7(b) shows the second phase, the post-ignition or the fast burn phase of the cookoff process. During this phase, the effect of the gap becomes more pronounced as the level of thermal explosion appears to depend on the pre-ignition condition of the system. The strain rates or the slopes of each curve shown in the figure are different for conditions with and without a gap. If one associates strain rates with flying particles or fragment velocities, the system without gap is clearly marked by a more violent reaction while the system with gap experiences a relatively less violent or benign response. Although the calculations probably provide a good estimate of the effects of the gap, the accuracy remains to be verified with a mesh refinement study.

5.3. TWO-DIMENSIONAL ANALYSIS

Two dimensional simulations are performed for the STEX system shown in Figures 1(b) and 4(b). This system is assumed to be axisymmetric, and a cylindrical wedge was selected for the calculation domain. In Figure 5, the calculated thermal response of the STEX system is shown together with measured data. In Figure 5, measured and calculated temperatures are shown at an internal location (no. 6 in Figure 1(b)) and the control location (no. 1 in Figure 1(b)). The measured and calculated thermal responses for the internal location generally agree except that the calculated ignition temperature is higher than the measurement by 5 degrees. These calculations were performed with the 8X mesh and are believed to be numerically accurate to less than a degree based on earlier mesh refinement studies. The differences between the model and measured results are likely the result of inaccuracies in the chemical kinetics models.

A series of temperature and pressure fields are shown in Figures 9 and 10 for the 8X mesh during the explosive stage of the cookoff process. The hot area in the center of the temperature field at $t = 0$ microseconds is the ignition point. The burn front advances outward into relatively cold solid explosive generating product gases. The resulting high pressures (see Figure 10) drive the steel vessel wall outward. It is also seen that there are irregularities in the burn front, and the temperature fields show complex structure throughout the interior product



Figure 9. Sequence of calculated temperature fields during expansion phase. Deflagration front separates the unburnt from the burnt regions of PBXN-109. The time is measured from the beginning of the burning phase, and temperatures range from 149 (blue) to 2327 °C (red). Model 2Da is used with the 8X mesh.

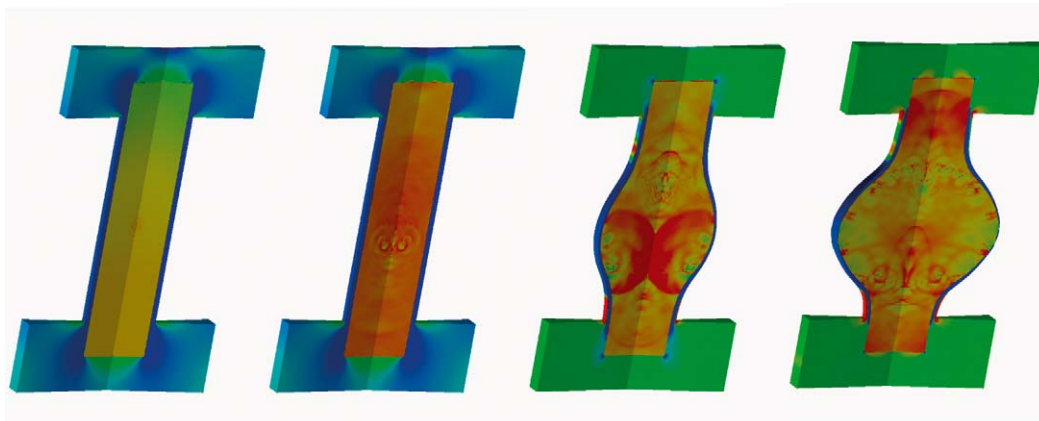


Figure 10. Sequence of calculated pressure fields during expansion phase. Hot product gases form a series of compressive and rarefaction waves inside the burning STEX vessel. The time is measured from the beginning of the burning phase, and pressures range from 0.1 (blue) to 200 MPa (red). Model 2Da is used with the 8X mesh.

gas region. A comprehensive analysis of the wave structure seen in the simulations is beyond the scope of this paper. However, we can still identify the waves in the gaseous HE as those described by the compressible Euler flow physics. The wave motion in the unburnt HE as well as in the steel is much more complex, and the ‘ringing’ effects seen in these regions are the high-frequency responses of metals and HE under mechanical and thermal stimuli as discussed in [35]. Although these fields are not likely to be fully resolved, it is expected that the fine mesh used captures much of the lower frequency behavior. It is also noted that the case wall is likely to have fractured during this sequence of temperature fields. The current model does not include fracture, and the metal wall simply stretches. Work is in progress to include these effects in the models

In Figure 11(a), calculated wall hoop strains for the STEX system are shown with the measurements. As was done for the one-dimensional case, the theoretical expansion of the empty steel vessel is plotted as well. Shown are the hoop strains for Model 2Da (side gap present) on meshes of four different resolutions. These results are generally higher than the

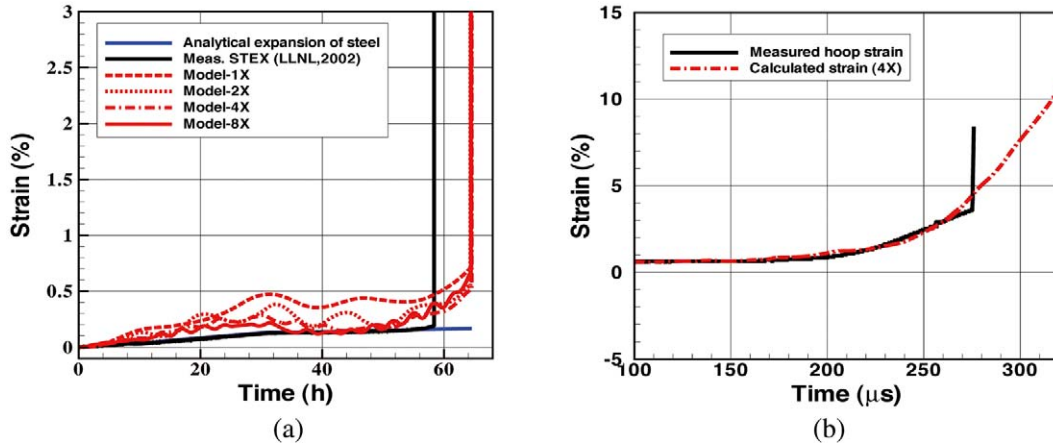


Figure 11. Calculated mechanical response of confined HE in a 2D STEX experiment. (a) The slow heating phase and ignition for Model 2Da. Four levels of mesh refinement are shown with an ideal steel expansion and the measurement. (b) Comparison of measured and calculated hoop strains during a thermal runaway for Model 2Db. The experimental strain data is available until about 275 μs when the gauge breaks.

measurements, and show spurious oscillations. Both of these numerical artifacts result from the method of mass scaling used in the integration of the momentum equations. The large calculated strains are the result of reduced sound speeds from mass scaling. The HE pressurizes the vessel before there is time for the explosive to expand upwards into the gap region near the top of the vessel. If the mass scaling is reduced, the upward expansion occurs faster, there is less pressurization, and the tube wall strains are reduced [36]. The spurious oscillations are similar to those observed for a simple harmonic oscillator in which the motion of the high mass material is guided by the restoring force of material elasticity. As the mass scaling is reduced, the amplitude and frequency of the oscillations increase. The results for the four meshes appear to be approaching a converged solution, but full convergence has not yet been achieved at 8X mesh resolution. The results for Model 2Da should match the empty vessel results until the 1% gap at the side of the HE cylinder closes at $t = 9.4$ hours with strain of 0.056%. It is seen that the Model 2Da curves are higher than the empty vessel curve during this period, indicating that numerical errors on the scale of 0.1% remain. Mesh refinement provides a better representation of the HE/air interface near the vessel wall. The remaining errors are attributed to the mass-scaling effects described above. It is important to minimize these errors since the state of the system prior to ignition can have a strong influence on the violence of the expansion as was observed for the 1D model.

A rapid expansion of the vessel wall follows the slow heating and ignition phases. In Figure 11(b), wall strain results for Model 2Db (no side gap) are compared with the measured hoop strain results for the STEX test. Shown are the calculated strain using the 4X mesh and the measurement. The model results compare favorably with the measured results until $t = 275 \mu\text{s}$. At this time, the measured strain rate changes dramatically. It is likely that the gauge failed at this point. Just prior to the gauge failure, the measured strain rate is approximately 400 s^{-1} , suggesting relatively low violence consistent with the relatively long time scale of the test and the fragmentation results discussed above.

Although the model provides a good representation of the measurements, mesh refinement results need to be completed to establish the numerical accuracy of the calculations. Also noted is the challenge to minimize the inherent oscillatory artifacts associated with mass

scaling. Oscillation-free strain results are possible if an implicit approach is used during the quasi-static process. To generate the smooth looking strain results of Figure 11(b), the time step size before the burn was reduced by a factor of 10^3 . To overcome this barrier, the implicit hydro approach is being developed for future calculations. Finally, the gap at the side of the HE needs to be added to provide a more complete model of the actual STEX system.

6. Conclusions

Progress has been made towards a predictive model for cookoff tests. Numerical procedures have been developed to model the thermal, mechanical, and chemical behavior during the slow heating, transition, and explosive phases in a single simulation. In this paper, attention is focused on the accuracy of mechanical results for the simulation of a thermal explosion test with PBXN-109. For the heating phase, an explicit hydro scheme with mass scaling provides numerically accurate results for wall strains in one-dimension and approximate results in two dimensions. The one-dimensional results show increased strain rates for the case of no gap. This result illustrates the importance of accurately modeling thermal, chemical, and mechanical behavior of the explosive system prior to ignition. For the rapid expansion, the 2D model provides a good representation of measured wall strains. However, a better treatment of gaps is needed during the heating phase to confirm the numerical accuracy of these model results. An implicit hydro scheme with slide surfaces is being developed to provide improved accuracy for cookoff systems with gaps.

Acknowledgements

Support for this work was provided by the DoD/DOE Joint Technology Development Program. The work was performed under the auspices of the U.S. Department of Energy by the University of California, Lawrence Livermore National Laboratory under Contract No. W-7405-Eng-48.

Authors would like to thank Albert Nichols for developing the ALE3D chemistry capability needed for the thermal explosion simulation. Discussions with Rich Becker on strain allocation model and with Brad Wallin on slide surfaces are greatly appreciated.

References

1. Mair, H. U., 'Review: Hydrocodes for Structural Response to Underwater Explosions', *Shock and Vibration*, **6**, pp. 81–96, 1999.
2. McGlaun, J. M., Yarrington, P., Asay, J. R., and Shahinpoor, M., (Eds.) High Pressure Shock Compression of Solids, *Large Deformation Wave Codes*, Springer-Verlag, 1993.
3. Anderson, Jr., C. E., 'An Overview of the Theory of Hydrocodes', *Int. J. Impact Engineering*, **5**, pp. 33–59, 1987.
4. McGlaun, J. M., Thompson, S. L., and Elrick, M. G., 'CTH: a Three-dimensional Shock Wave Physics Code', *Int. J. Impact Engineering*, **10**, pp. 351–360, 1990.
5. Mandell, D. A., Adams, T. F., Mosso, S. J., Holian, K. S., Addessio, F. L., and Baumgardner, J. R., 'MESA: a 3-D Computer Code for Armor/Anti-Armor Applications', Los Alamos National Laboratory, Report LA-UR-89-1263, 1989.
6. Quirk, J. J., 'A Parallel Adaptive Grid Algorithm for Computational Shock Hydrodynamics', *Applied Numerical Mathematics*, **20**, pp. 427–453, 1996.

7. Stewart, D. S., Aslam, T., Yao, J., and Bdzil, J. B., 'Level-set Techniques Applied to Unsteady Detonation Propagation', in *Modeling in Combustion Science, Proceedings, Springer-Verlag*, pp. 352–369, Berlin, Germany, 1995.
8. Bourlioux, A., and Majda, A. J., 'Theoretical and Numerical Structure for Unstable Two-Dimensional Detonations', *Combustion and Flame*, **90**, pp. 211–229, 1992.
9. Oran, E. S., Boris, J. P., Young, T., Flanagan, M., Burks, T., and Picone, M., 'Numerical Simulations of Detonations in Hydrogen-Air and Methane-Air Mixtures', in *Proceedings of 18th Symposium on Combustion*, The Combustion Institute, 1981, pp. 1641–1649.
10. McClelland, M. A., Maienschein, J. L., Nichols, A. L., Wardell, J. F., Atwood, A. I., and Curran, P. O., 'ALE3D Model Predictions and Materials Characterization for the Cookoff Response of PBXN-109', in *Proceedings of JANNAF 38th Combustion and 20th Propulsion Systems Hazards Subcommittee Meetings*, Destin, FL, 2002.
11. McClelland, M. A., Tran, T. D., Cunningham, B. J., Weese, R. K., and Maienschein, J. L., 'Cookoff Response of PBXN-109: Material Characterization and ALE3D Thermal Predictions', in *Proceedings of JANNAF 50th Propulsion Meeting*, Salt Lake City, UT, 2001.
12. McClelland, M. A., Maienschein, J. L., Nichols, A. L., and Yoh, J. J., 'Joint DoD/DOE Munitions Technology Development Program FY-02 Report, Ignition and Initiation Phenomena: Cookoff Violence Prediction', UCRL-ID-103482-02, 2002.
13. Wardell, J. F., and Maienschein, J. L., 'The Scaled Thermal Explosion Experiment', in *Proceedings of 12th International Detonation Symposium*, San Diego, CA, Office of Naval Research, 2002.
14. Nichols, A. L., Couch, R., McCallen, R. C., Otero, I., and Sharp, R., 'Modeling Thermally Driven Energetic Response of High Explosives', in *Proceedings of 11th International Detonation Symposium*, Snowmass, Colorado, pp. 862–871, 1998.
15. Yoh, J. J., and McClelland, M. A., 'Simulating the Thermal Response of High Explosives on Time Scales of Days to Microseconds', in *Proceedings of 13th APS SCCM Conference*, Portland, Oregon, 2003.
16. Yoh, J. J., McClelland, M. A., Maienschein, J. L., Nichols, A. L., and Wardell, J. F., 'Towards an Ideal Cookoff Model for PBXN-109', in *Proceedings of JANNAF 21st Propulsion Systems Hazards Subcommittee Meetings*, Colorado Springs, Colorado, 2003.
17. Chidester, S. K., Tarver, C. M., Green, L. G., and Urtiew, P. A., 'On the Violence of Thermal Explosion in Solid Explosives', *Combustion and Flame*, **110**, pp. 264–280, 1997.
18. Tarver, C. M., and Tran, T. D., 'Thermal Decomposition Models for HMX-based Plastic Bonded Explosives', *Combustion and Flame*, **137**, pp. 50–62, 2004.
19. Baer, M. R., Hobbs, M. L., Gross, R. J., and Schmitt, R. G., 'Cookoff of Energetic Materials', in *Proceedings of 11th International Detonation Symposium*, Snowmass, Colorado, Office of Naval Research, pp. 852–861, 1998.
20. Matheson, E. R., Drumheller, D. S., and Baer, M. R., 'A Coupled Damage and Reaction Model for Simulating Energetic Material Response to Impact Hazards', in *Proceedings of APS SCCM Conference*, Snowbird, Utah, pp. 651–654, 1999.
21. Schmitt, R. G., Erikson, W. W., Away, B., Dickson, P., Henson, B., Smilowitz, L., and Tellier, L., 'Application of a Multiphase Mixture Theory with Coupled Damage and Reaction to the LANL Large-Scale Annular Cookoff Experiment', in *Proceedings of JANNAF 19th Propulsion Systems Hazards Subcommittee Meetings*, Monterey, CA., 2000.
22. Atwood, A. I., Curran, P. D., Lee, K. B., and Bui, D. T., 'Experimental Progress on a Cookoff Model Validation Effort', in *Proceedings of JANNAF 38th Combustion and 20th Propulsion Systems Hazards Subcommittee Meetings*, Destin, FL, 2002.
23. Sandusky, H. W., and Chambers, G. P., 'Validation Experiments for Slow Cookoff', in *Proceedings of JANNAF 38th Combustion and 20th Propulsion Systems Hazards Subcommittee Meetings*, Destin, FL, 2002.
24. Erikson, W. W., and Schmitt, R. G., 'Pre- and Post-ignition Modeling of Validation Cookoff Experiments', in *Proceedings of JANNAF 38th Combustion and 20th Propulsion Systems Hazards Subcommittee Meetings*, Destin, FL, 2002.
25. Belytschko, T., 'An Overview of Semidiscretization and Time Integration Procedures', in *Computational Methods for Transient Analysis*, edited by T. Belytschko and T. J. R. Hughes, North-Holland, 1983, pp. 1–65.
26. Sharp, R., and the ALE3D Team, *Users Manual for ALE3D*, Lawrence Livermore National Laboratory, Ver. 3.6.1, October 25, 2003.

27. McGuire, R. R., and Tarver, C. M., 'Chemical Decomposition Models for the Thermal Explosion of Confined HMX, TATB, RDX, and TNT Explosives', in *Proceedings of 7th International Detonation Symposium*, Annapolis, MD, Naval Surface Weapons Center, 1981, pp. 56–64.
28. Steinberg, J., 'Equation of State and Strength Properties of Selected Materials', UCRL-MA-106439, 1991.
29. Catalano, E., McGuire, R., Lee, E. L., Wrenn, E., Ornellas, D., and Walton, J., 'The Thermal Decomposition and Reaction of Confined Explosives', in *Proceedings of 6th International Detonation Symposium*, Coronado, CA, Office of Naval Research, pp. 214–222, 1976.
30. Tran, T. D., 'A Compilation of One-Dimensional, Time-To-Explosion (ODTX) Test Data for High Explosives and Propellants', UCRL-ID-151449, 2003.
31. Atwood, A. I., Personal communication, NAWC-CL, 2001.
32. Maienschein, J. L., and Wardell, J. F., 'Deflagration Rate of PBXN-109 and Composition B at High Pressures', in *Proceedings of JANNAF 38th Combustion and 20th Propulsion Systems Hazards Subcommittee Meetings*, Destin, FL, 2002.
33. Holman, J. P., *Heat Transfer*, McGraw-Hill, 1976, pp. 253–254.
34. Prior, A. M., 'Applications of Implicit and Explicit Finite Element Techniques to Metal Forming', *J. of Material Processing Technology*, **45**, pp. 649–656, 1994.
35. Meyers, M. A., *Dynamic Behavior of Materials*, John Wiley & Sons, Inc., New York, NY, 1994.
36. McClelland, M. A., Maienschein, J. L., Reaugh, J. E., Tran, T. D., Nichols, A. L., and Wardell, J. F., 'ALE3D Model Predictions and Experimental Analysis of the Cookoff Response of Comp B', in *Proceedings of JANNAF 21st Propulsion Systems Hazards Subcommittee Meetings*, Colorado Springs, Colorado, 2003.